Please find the published version at: https://doi.org/10.1016/j.applthermaleng.2021.116748

Wet steam flow and condensation loss in turbine blade cascades

Chuang Wen[1], Yan Yang[1*], Hongbing Ding[2], Chunqian Sun[2], Yuying Yan[1, 3*]

[1]Faculty of Engineering, University of Nottingham, Nottingham NG7 2RD, United Kingdom

[2]School of Electrical and Information Engineering, Tianjin University, Tianjin 300072, China

[3]Research Centre for Fluids and Thermal Engineering, University of Nottingham Ningbo China, Ningbo 315100, China

*Corresponding author: Yan Yang, yanyang2021@outlook.com

Yuying Yan, yuying.yan@nottingham.ac.uk

Abstract: This study develops a wet steam modelling to solve the phase change process inside the blade cascade of a steam turbine. The comparative study is carried out to understand the impact of the dry gas model and wet steam model on predicting the flow behaviours in a steam turbine. The effect of the cutback of the trailing edge on the flow structure and nonequilibrium condensation is evaluated in blade cascades. The results show that the dry gas assumption without considering the phase change process predicts fraudulently flow separations near the trailing edge to induce oblique waves. The maximum liquid fraction can reach approximately 0.051 based on the wet steam flow modelling. The condensation-evaporation processes in the blade cascades cause a condensation loss of 0.118 MW. The stronger expansion flow is obtained to induce the earlier onset of the homogeneous nucleation process with an increasing cutback of the trailing edge. The 21% cutback of the trailing edge leads to strong flow separations on

the suction side to severely deteriorate the flow condition in blade cascades. It suggests that the cutback of the trailing edge by 14% is acceptable to repair damaged blades considering the flow structure, nonequilibrium phase change and condensation loss.

Keywords: wet steam, nonequilibrium condensation, condensation loss, steam turbine, turbine blade, trailing edge

Nomenclature

CFD	computational fluid dynamics	r	droplet radius, m
SST	shear stress transport	r_c	critical droplet radius, m
a	experimental value	R^2	root-mean-square, -
b	numerical value	R_v	gas constant, $J \cdot K^{-1} \cdot mol^{-1}$
E	total energy, J kg^{-1}	S	degree of supersaturation, -
h_{fg}	latent heat, J kg^{-1}	t	time, s
J	nucleation rate, m^{-3} s^{-1}	T	temperature, K
k_B	Boltzmann's constant, 1.38×10^{-23} J K^{-1}	u	velocity, $m \cdot s^{-1}$
		V_d	droplet volume, m^3
Kn	Knudsen number, -	x	Cartesian coordinates, m
Ldr	condensation loss, MW	y	liquid fraction, -
m_1	mass generation rate due to nucleation process, kg m^{-3} s^{-1}	β	modelling parameter, -
		γ	specific heat ratio, -
m_2	mass generation rate due to droplet growth process, kg m^{-3} s^{-1}	ΔG	Gibbs free energy, J
		ΔT	subcooling, K
m_{in}	liquid flow rate at the inlet boundary, kg s^{-1}	λ_v	vapour conductivity, $W \cdot m^{-1} \cdot K^{-1}$
		ν	modelling correction coefficient, -
m_{out}	liquid flow rate at the outlet boundary, kg s^{-1}	ρ	density, kg m^{-3}
		σ	surface tension, $N \cdot m^{-1}$
m_v	mass of a vapour molecule, kg	τ_{ij}	viscous stress tensor, kg m^{-1} s^{-2}
N	droplet number per volume, m^{-3}	ϕ	temperature correction coefficient, -
p	pressure, Pa		
Pr	Prandtl number, -	c	critical condition
q_c	condensation coefficient, -	i, j	Cartesian tensor notation
q_{dr}	condensation loss coefficient, -	l	liquid phase
q_{jeff}	effective heat flux, W m^{-2}	s	saturation condition
		v	vapour phase

1. Introduction

The liquid phase inside the blade cascades of a steam turbine [1] can cause energy

losses and erosion-corrosion issues to reduce the reliability of the equipment [2, 3]. Therefore, one of the essentials is to understand the wet steam flow and condensation loss inside blade cascades. Bakhtar et al. carried out experimental measurements of turbine blades including the pressure distributions in the nucleation steam [4], and the pressure distribution [5] and droplet sizes [6] in wet steam flows. White et al. [7] proposed and designed an experimental rig to measure the blade wall pressures and Schlieren flow pictures in a steam turbine. Yousif et al. [8] experimentally investigated the nonequilibrium condensations inside low-pressure steam turbine cascades, and the pressure distribution and isentropic Mach number were measured on pressure and suction sides. Dykas et al. [9-11] performed the experimental studies in the blade cascade to identify the blade surface pressure distributions and obtained the Schlieren pictures of the flow structures inside the steam turbines.

The computational fluid dynamics (CFD) modellings were developed to study flow features inside steam turbines[12, 13]. Bakhtar et al. [14] studied Runge-Kutta and Denton time-marching computational schemes on the prediction of the nucleation flows inside a steam turbine and they suggested that the two schemes agreed well with experimental data. Wróblewski et al. [15] utilised a condensing flow modelling to study Laval nozzles, two-dimensional and three-dimensional turbine blades and they found that the predicted condensed droplets were smaller than the experimental tests in low-pressure conditions, which were larger for high-pressure steams. Ding et al. [16] investigated the entropy and exergy issues in a steam turbine in the presence of surface roughness and they reported that the increasing roughness caused the increase of the

entropies and exergy destructions. Vatanmakan et al. [17] numerically studied the entropy generations in a steam turbine in the presence of the condensing flows and they showed that the condensation could be reduced via heating the blade surfaces. Zhang et al. optimised the steam turbine blade by inserting a flow channel into the blade and they found that the condensation region could be reduced to improve the blade performance [18-21]. Dykas & Wróblewski [22] developed a two-fluid condensing flow modelling to solve separately vapour phase and liquid phase governing equations and they observed velocity slips between these two phases in the steam turbine. Han et al. [23] proposed a two-fluid condensing flow modelling to clarify the influences of the surface heating on blade performances and their numerical investigation showed that the surface heating could restrain the nonequilibrium condensations in the steam turbines. Ebrahimi-Fizik et al. [24] used the non-uniform rational B-splines mesh generation methods to investigate the wet steam flows in a steam turbine and they reported that the prediction of pressure and droplet radius could be improved by 35.64% and 78.44%, respectively. Cao et al. [25] investigated the condensed droplet distribution in a three-dimensional steam turbine, and they found that the vortexes could influence the locations, numbers and sizes of the condensed droplets in the steam turbine. Yazdani & Lakzian [26], Ding et al. [27] employed the Eulerian-Lagrangian method to solve the nonequilibrium condensation in steam turbines.

With the great effort of the aforementioned studies, the phase change of the steam in the blade cascade still needs to be further investigated. Considering the literature survey, the novelty and contents of this work are:

(1) A two-phase wet steam modelling is developed to evaluate nonequilibrium condensations inside steam turbines. The qualitative and quantitative analyses are carried out to study the effect of the dry gas and wet steam models on predicting flow features in turbine blades. Specifically, the evaporation of the condensed droplets is revealed and the condensation loss is investigated considering the condensation-evaporation processes.

(2) The trailing edge of the steam blades may suffer deterioration due to the particles in the wet steam flow and one of the typical repair methods is to cut back the trailing edge [28]. The effect of the cutback of the trailing edge on the blade performance is evaluated using the wet steam flow model. The nonequilibrium condensation and condensation loss are discussed in different cutback levels of the blade to show how the cutback of the trailing edge affect the flow structure in the blade cascades.

This work provides a detailed and quantitative evaluation of the nonequilibrium condensation of steam in turbine blade cascade, and the effect of the cutback of the trailing edge on the blade performance is evaluated. This will be useful for the design and operation of a steam turbine and provides an understanding of fluid dynamics and thermal process for the application of a steam turbine.

2. Mathematical modelling

2.1. Governing equations

The Eulerian- Eulerian approach is employed for a steam turbine assuming that the spontaneous condensation is considered without involving external solid impurities/particles in the numerical simulation [29, 30]. The unsteady compressible

conservation equations of mass, momentum and energy are employed to govern the two-phase wet steam flows inside a steam turbine [31, 32].

$$\frac{\partial \rho}{\partial t}+\frac{\partial(\rho \boldsymbol{u}_j)}{\partial x_j}=-(\dot{m}_1+\dot{m}_2) \tag{1}$$

$$\frac{\partial}{\partial t}\left(\rho \boldsymbol{u}_i\right)+\frac{\partial}{\partial x_j}\left(\rho \boldsymbol{u}_i \boldsymbol{u}_j\right)=-\frac{\partial p}{\partial x_i}+\frac{\partial \tau_{ij}}{\partial x_j}-\boldsymbol{u}_i(\dot{m}_1+\dot{m}_2) \tag{2}$$

$$\frac{\partial(\rho E)}{\partial t}+\frac{\partial}{\partial x_i}\left[\boldsymbol{u}_i(\rho E+p)\right]=\frac{\partial q_{jeff}}{\partial x_j}+\frac{\partial}{\partial x_j}(\boldsymbol{u}_i \tau_{ij})-h_{fg}(\dot{m}_1+\dot{m}_2) \tag{3}$$

Two scalar equations are utilised to describe nonequilibrium condensation processes in steam turbines [33, 34]:

$$\frac{\partial(\rho y)}{\partial t}+\frac{\partial\left(\rho y u_i\right)}{\partial x_i}=\dot{m}_1+\dot{m}_2 \tag{4}$$

$$\frac{\partial(\rho N)}{\partial t}+\frac{\partial\left(\rho N u_i\right)}{\partial x_i}=\rho J \tag{5}$$

where y and N are the liquid fraction and droplet numbers during the nonequilibrium condensation process in transonic flows [35].

2.2. Spontaneous condensation

During the spontaneous condensation process in transonic flows, the molecular clusters need to overcome the free critical energy barriers to form a droplet without the existence of external seeds, which contains the homogeneous nucleation process and droplet growth process. With the assumption of a spherical droplet, the Gibbs free energy can be expressed as:

$$\Delta G=4\pi r^2 \sigma-\frac{4}{3}\pi r^3 \rho_l R_v T_v \ln(S) \tag{6}$$

The critical radius of a droplet can be obtained when the Gibbs free energy reaches the maximum value:

$$r_c = \frac{2\sigma}{\rho_l R_v T_v \ln(S)} \tag{7}$$

$$S = \frac{p_v}{p_s} \tag{8}$$

The classical nucleation theory is employed here to describe the homogeneous nucleation rate, J [36], which is given by

$$J = \frac{q_c}{1+\phi}\frac{\rho_v^{\,2}}{\rho_l}\sqrt{\frac{2\sigma}{\pi m_v^{\,3}}}\exp\left(-\frac{4\pi\sigma}{3k_B T_v}r_c^{\,2}\right) \tag{9}$$

where ϕ is the temperature correction coefficient:

$$\phi = 2\frac{\gamma-1}{\gamma+1}\frac{h_{fg}}{R_v T_v}\left(\frac{h_{fg}}{R_v T_v}-\frac{1}{2}\right) \tag{10}$$

The droplet growth rate dr/dt [37, 38] is calculated by:

$$\frac{dr}{dt} = \frac{\lambda_v \Delta T}{\rho_l h_{fg} r}\frac{\left(1-r_c/r\right)}{\left(\frac{1}{1+2\beta\mathrm{Kn}}+3.78(1-\nu)\frac{\mathrm{Kn}}{\mathrm{Pr}}\right)} \tag{11}$$

$$\Delta T = T_s - T_v \tag{12}$$

The liquid mass generation rates per volume during the phase change process includes $\dot{m}_1$ (kg s^{-1} m^{-3}) contributed by the homogenous nucleation process and $\dot{m}_2$ (kg s^{-1} m^{-3}) contributed by the droplet growth process.

$$\dot{m}_1 = \frac{4}{3}\pi r_c^{\,3}\rho_l J \tag{13}$$

$$\dot{m}_2 = 4\pi r^2 \rho_l N \frac{dr}{dt} \tag{14}$$

The relationship between the liquid fraction and numbers of liquid droplets can be expressed as:

$$N = \frac{y}{(1-y)V_d\left(\rho_l/\rho_v\right)} \tag{15}$$

$$V_d = \frac{4}{3}\pi r^3 \tag{16}$$

where V_d is the droplet volume.

The thermodynamic parameters are crucial to calculate the physical properties of water vapour during the nonequilibrium condensation in supersonic flows. In this numerical simulation, the REFPROP database NIST model [39] is employed to predict the water vapour properties. The NIST real gas model accurately represents the thermodynamic properties in the temperature range of 251.165 - 2000 K and for pressures up to 1000 MPa, which has been employed for the prediction of nonequilibrium condensations in supersonic flows [40].

2.3. Numerical implementation

For the modelling implementation, the two scalar equations (4) and (5), and source terms in equations (6) - (17) are interpreted by the C programming [41, 42] and are integrated into ANSYS FLUENT 18. The density-based approach is employed to solve the wet steam flow in steam turbines, and the second-order upwind discretization is used for the flow, turbulence and droplet number and liquid fraction equations. The thermophysical properties like the density [43], viscosity [44], specific heat capacity [45] and thermal conductivity [46] are used for the steam. The k-ω SST turbulence modelling [47, 48] is utilized for solving the steam turbine based on its accuracy for the condensing process [49] in transonic flows [50]. The turbulent intensity and turbulent viscosity ratio are chosen at the inlet (5% and 10 in this study) and outlet (10% and 10 in this study) boundaries. The inlet velocity direction is set perpendicular to the inlet boundary and the outlet velocity direction is calculated from the upstream neighbouring

cell. The convergence criteria in this study are below 1.0×10^{-4} for all dependent variables and the relative difference of mass flow rate between the inlet and out boundaries is lower than 0.0005%.

2.4. Physical model

The steam blade in Bakhtar et al experiments [51] is used here for the numerical simulation, as shown in Fig. 1. The axial chord and pitch of the blade are 25.27 mm and 18.26 mm, respectively. The boundary conditions for the numerical simulations are described in Fig. 1, including the pressure inlet for the entrance, pressure outlet for the exit, the periodic boundary for upstream and downstream regions of the blades, no-slip and adiabatic walls for the pressure side and suction side.

The structured quadrilateral mesh is generated for the blade cascade using ANSYS ICEM CFD. The mesh independent tests are studied based on four different grid densities including 8800 (coarse), 22400 (medium), 45600 (fine) and 92800 (refined) cells. The wall pressure on the steam blade cascade in Fig. 2 (a) and the nucleation rate along the flow direction in Fig. 2 (b) are compared in detail. The static pressure downstream the nucleation process is over-predicted by the coarse mesh compared to the medium, fine and refined meshes. Also, the coarse mesh predicts the earlier onset of the nucleation rate than the other three cases. The fine and refined meshes calculate similar wall pressure and nucleation rates than the medium one. Therefore, the fine mesh of 45600 cells is used for wet steam flows inside the steam blade considering computational accuracy and costs.

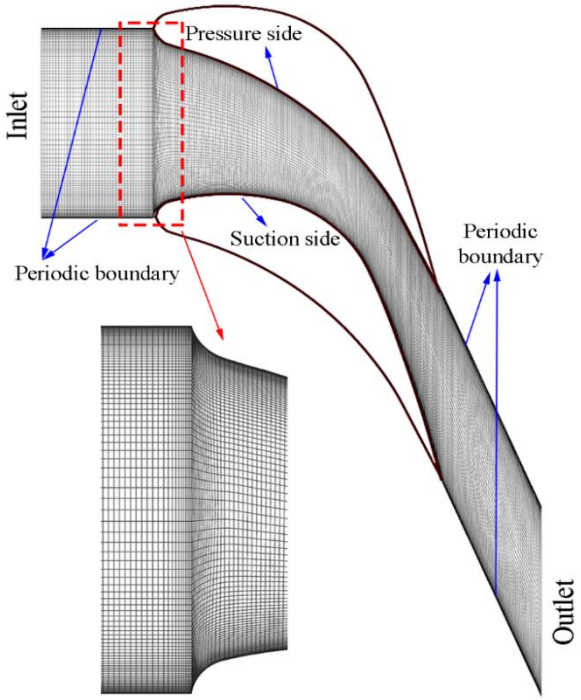

Fig. 1 Geometry, boundary conditions and computational grid of the steam blade in Bakhtar et al experiments [51]

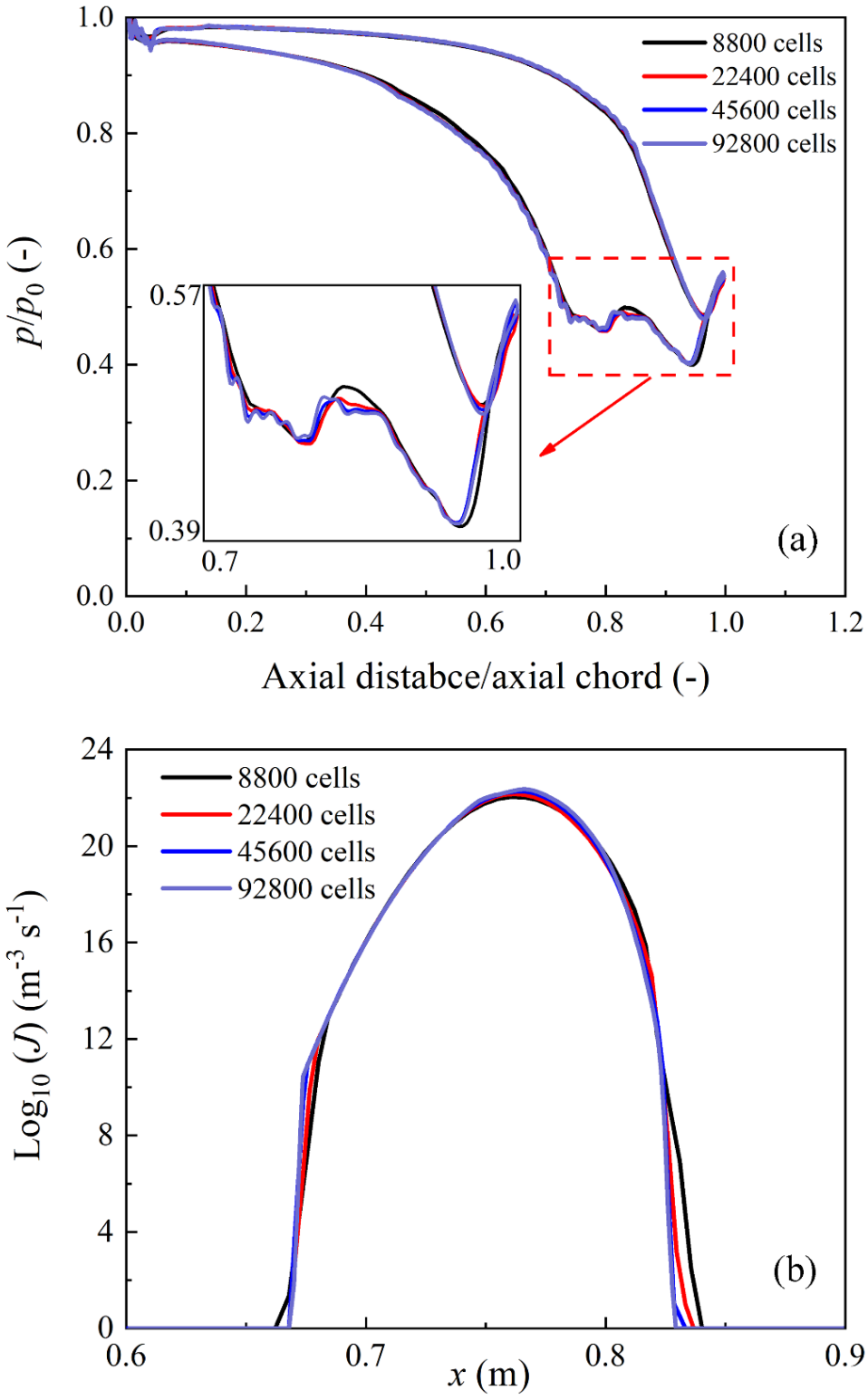

Fig. 2 Flow behaviour in a steam turbine with four grid densities: blade wall pressures (a) and nucleation rate along the flow direction (b)

3. Results and discussion

3.1. Validation of wet steam flow in supersonic nozzles

A supersonic nozzle [52] is first employed to validate the wet steam modelling. The detailed geometry, size and mesh can be found in Fig. 3 (a) and (b). The root-mean-square (R^2) defined in Eq. (17) is used to evaluate the errors between numerical and experimental results [53-55]. The comparison results and error analysis are shown in Fig. 3 (c) and (d). The numerical pressures agree well with experimental data with the root-mean-square (R^2) of approximately 0.9990. The relative error between the numerical and experimental droplet radius is 5.94%. Furthermore, the expansion line at the central line of the supersonic nozzle is described in the enthalpy-entropy diagram considering the nonequilibrium condensations in supersonic flows, as shown in Fig. 4. The comparison between the expansion line and saturation line illustrates that the steam presents dramatically nonequilibrium state to induce the phase change in supersonic flows. The enthalpy-entropy line further validates the accuracy of the thermodynamic properties in modelling the nonequilibrium condensation in supersonic flows. Thus, the developed CFD model accurately predicts the flow feature of the steam condensation in supersonic flows.

$$R^2 = 1 - \frac{\sum_{i=1}^{n} (a_i - b_i)^2}{\sum_{i=1}^{n} (b_i)^2} \tag{17}$$

where a_i and b_i are experimental and numerical values.

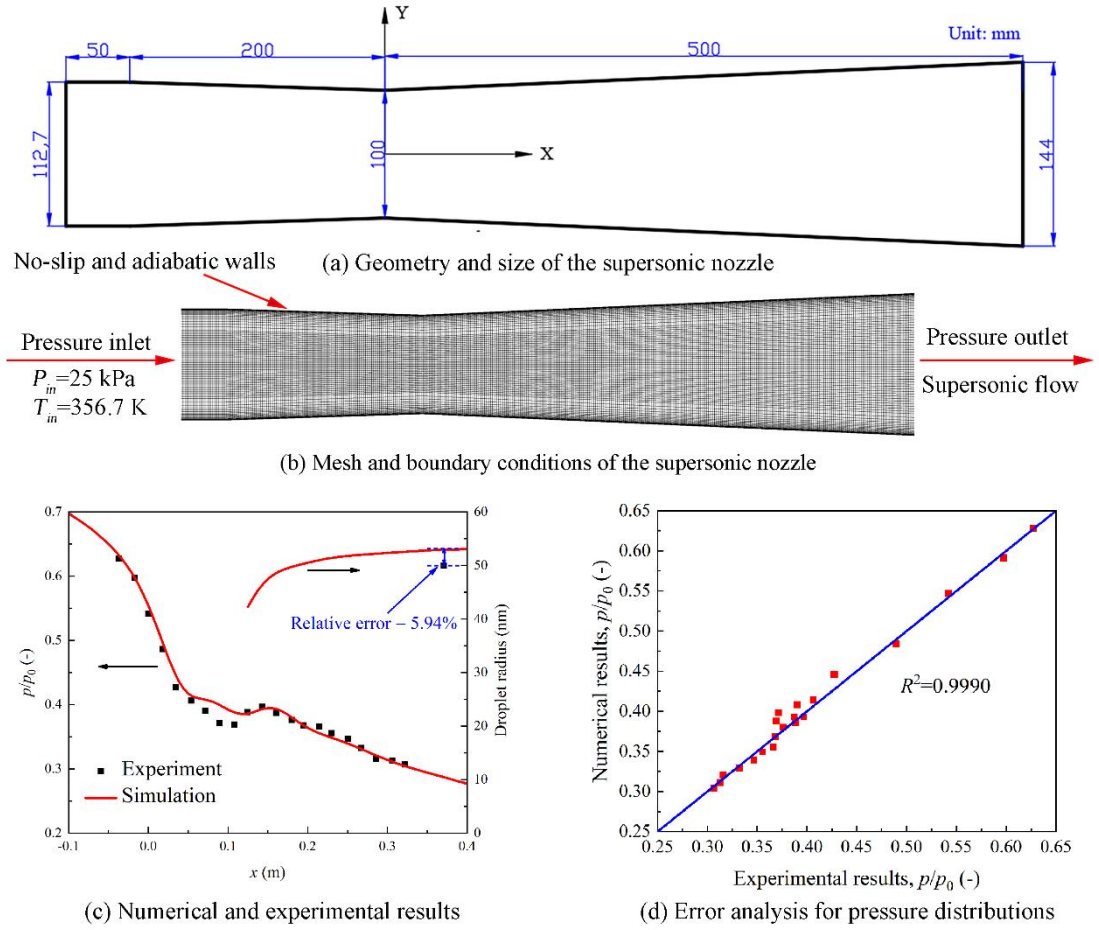

Fig. 3 Geometry, mesh, boundary conditions, numerical and experimental results, and error analysis of wet steam flow in a supersonic nozzle

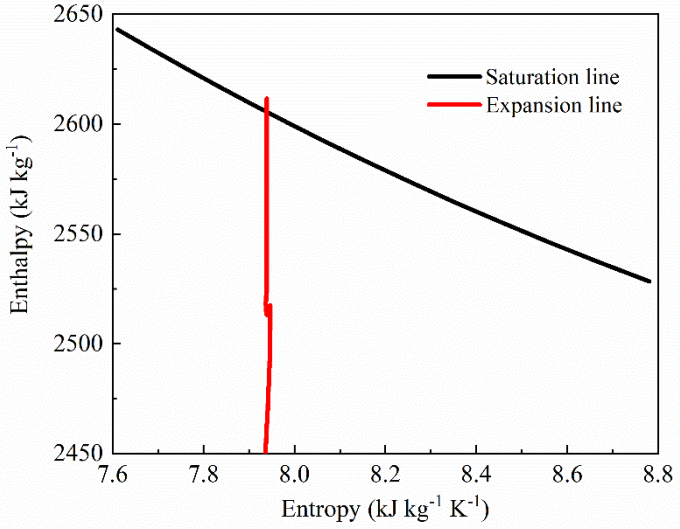

Fig. 4 Enthalpy-entropy diagram at the central line of the Moore et al. nozzle [52] considering the nonequilibrium condensation process

3.2. Validation of wet steam flow in turbine blades

This section further validates the wet steam modelling for a steam blade in Bakhtar et al experiments [51]. In the experimental tests, the pressure distributions are tested on blade surfaces and the droplet sizes are measured at the exit. Figure 5 describes the numerical and experimental wall pressures and droplet sizes. The root-mean-square (R^2) of the wall pressure between experiment and simulation is shown in Fig. 6. The developed wet steam model predicts good results for the pressure side and the root-mean-square (R^2) subsequently reaches 0.9950 although there are two large differences near the trailing edge. For the suction side, the CFD model agrees well with the experimental measurement in the upstream region of the condensation and accurately captures the condensation shock. In the near region downstream the condensation, the numerical wall pressures are lower than the experimental value. The R^2 between experimental and numerical pressures are approximately 0.9993 for the suction side. For the droplet size comparison, the experimental droplet radius is 0.057 μm at the blade cascade exit, while the numerical averaged droplet radius at the exit plane of the cascade is approximately 0.046 μm. The relative error between the experimental and numerical droplet radii is around 19.3% at the cascade exit. In general, the developed wet steam model can predict wet steam flows inside blade cascades of a steam turbine.

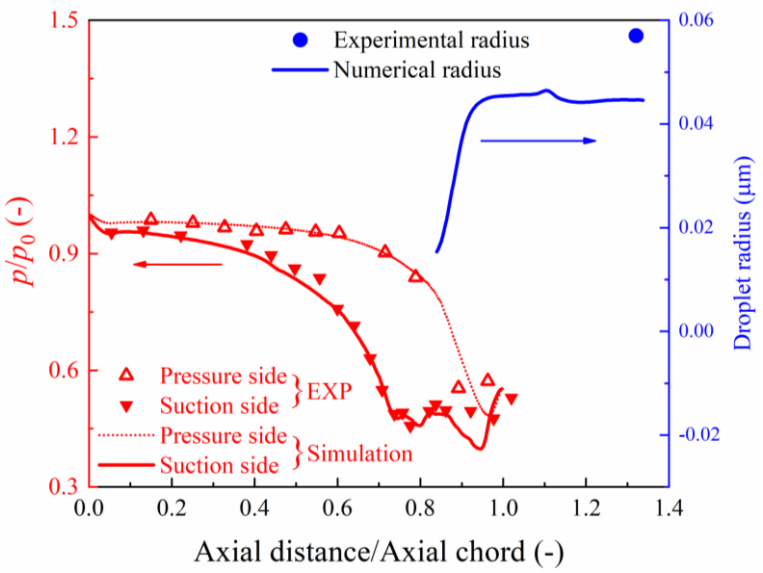

Fig. 5 Wall pressure and droplet radius in Bakhtar et al steam blades [51]

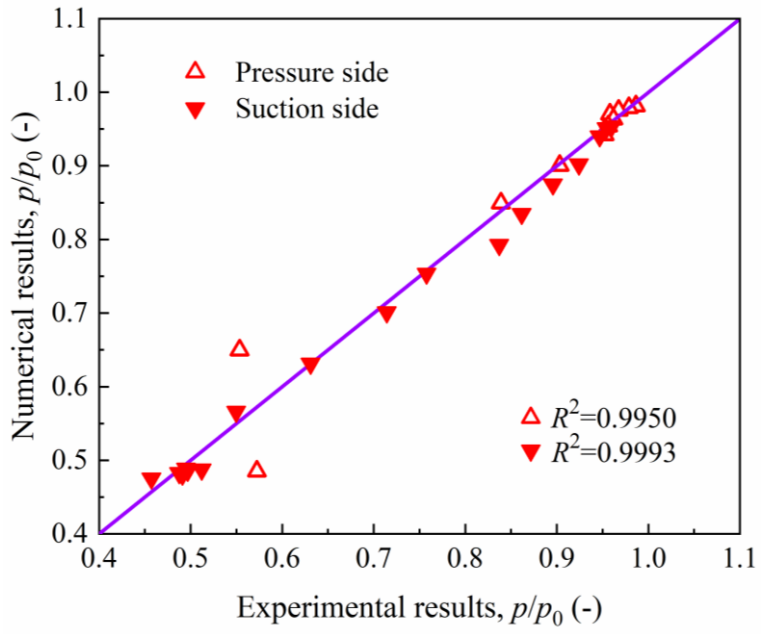

Fig. 6 Root-mean-square (R^2) between numerical and experimental wall pressures in Bakhtar et al steam blades [51]

3.3. Flow features in steam blade cascades

This section compares the dry gas model and wet steam model for predicting the flow structure inside blade cascades. The computational boundary condition is described in Table 1. Figure 7 shows the Mach number, static pressure and static

temperature in steam turbines. The dry gas model predicts a strong flow separation near the trailing edge, which is demonstrated by the steep pressure rise at x/x_{ch} = 0.828 in Fig. 7(d). The flow separation phenomenon further induces the complex oblique waves, which can be observed by the pressure contours in Fig. 7(a), temperature contours in Fig. 7 (b), Mach number contours in Fig. 7(c) and the profiles of the temperature and Mach number in Fig. 7(e). The reason is that the condensation processes weaken the steam expansion in supersonic flows and change the flow structure in the turbine blades. For the dry gas assumption, the Mach number is approximately 1.40 at the reflection point of the suction wall, where the Mach number is only 1.09 for the wet steam model as shown in Fig. 7(c). The interaction between the steam expansion flow and the suction wall of the blade generates the unrealistic phenomenon of the oblique waves in the dry gas model. The wet steam model predicts the nonequilibrium condensation when the supersonic flow is achieved inside blade cascades, which generates the condensation shock during phase change processes. As shown in Fig. 7(d), the Wilson point [56] of the nonequilibrium condensation is at x/x_{ch} = 0.859 and subsequently improve the flow structure near the trailing edge.

During the spontaneous condensation, the latent heat is released to induce a static pressure rise to form the condensation shock. Subsequently, the static temperature downstream the condensation shock by the wet steam modelling is dramatically higher than the dry gas modelling. The wet steam model predicts the static temperature downstream the condensation shock higher than 375 K, while the dry gas gives 324 K at x/x_{ch} = 1.113, where the temperature difference can reach 51 K. Furthermore, the wet

steam modelling computes a maximum Mach number of 1.16 compared to the maximum value of 1.41 for the dry gas model. It indicates that the dry gas model over-predicts expansion characteristics of the steam in the blade cascade of a steam turbine because it neglects the heat and mass transfer during nonequilibrium condensation processes.

Table 1 Boundary conditions for steam blade cascades

Boundary conditions	Blade inlet	Blade outlet	Fluid and walls
Total pressure	172000 Pa	83560 Pa	Wet steam flow
Total temperature	380.7 K	380.7 K	No-slip, adiabatic walls

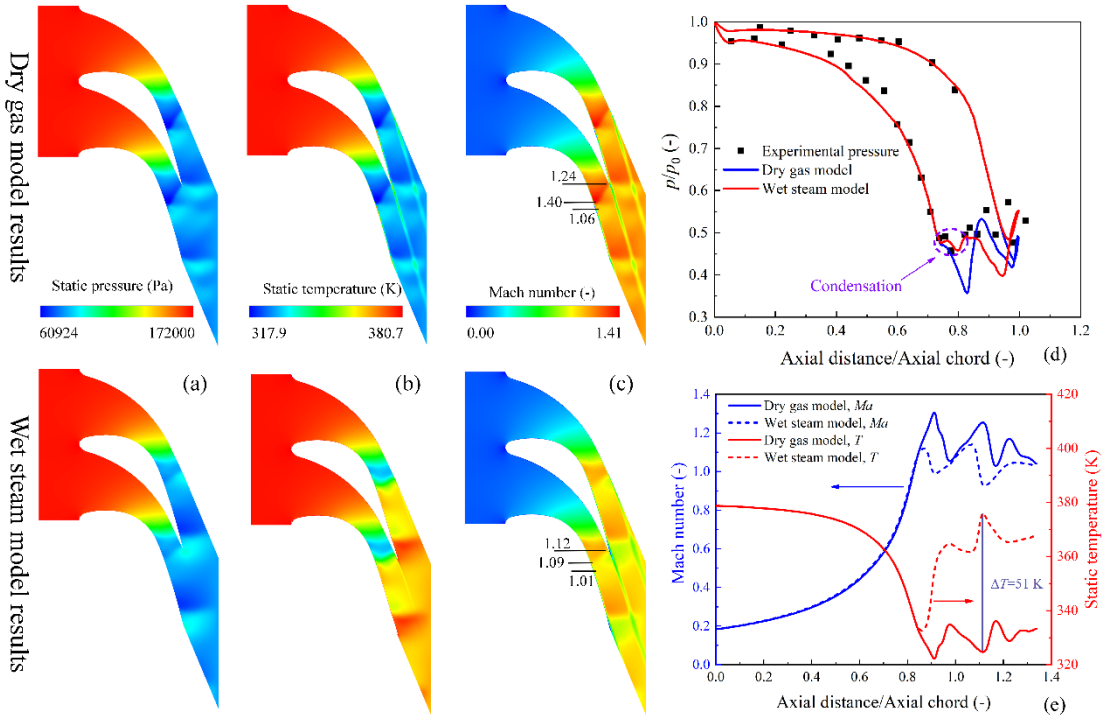

Fig. 7 Flow structures in the steam blade with dry gas and wet steam models: contours of the static pressure (a), contours of the static temperature (b), contours of the Mach number (c), profiles of the blade wall pressures (d) and profiles of the static temperature and Mach number at the middle line of the flow channel (e)

The nonequilibrium condensation processes inside blade cascades are shown in Fig. 8, including the degree of supercooling, nucleation rate, mass generation rate,

droplet radius, droplet number and liquid fraction, respectively. It can be seen that the degree of supercooling increased due to steam expansions inside the flow channel of blade cascades. The maximum degree of supercooling is approximately 37 K to form an extremely nonequilibrium state of the steam to generate the homogeneous nucleation process in the flow channel. The maximum value of the nucleation rate is 2.42×10^{22} m^{-3} s^{-1}, as shown in Fig. 8 (b). The degree of supercooling stays at around 7 K downstream the nucleation region to induce the droplet growth process, which generates a large amount of stable condensed droplets. The maximum droplet number can reach 7.57×10^{16} m^{-3} and the maximum droplet radius is approximately 0.053 μm inside blade cascades. The generation of the condensed droplets releases the latent heat to the vapour phase. The mass generation rate contributed by the homogeneous nucleation and droplet growth processes determines the heat and mass transfer during nonequilibrium condensations inside blade cascades for a steam turbine. In this simulation, we can see that the maximum value of the mass generation rate can reach 2374 kg m^{-3} s^{-1} in the close region downstream the trailing edge. Also, it can be observed that the mass generation rate represents -1161 kg m^{-3} s^{-1} further downstream the flow channel, which indicates that the condensed droplet evaporates into the vapour phase. This is also demonstrated by the distribution of the liquid fraction which achieves the peak value of approximately 0.051 in this case. The condensation and evaporation processes in the blade cascade increase the energy loss in a steam turbine.

Figure 9 illustrates the enthalpy-entropy distribution at the middle line in the flow region from the inlet to the blade outlet, which does not include the downstream flow

channel of the blade cascade. The expansion line demonstrates the supersaturation state at the inlet of the blade cascade with the given pressure and temperature conditions. The steam goes further to become an extremely nonequilibrium state due to the expansion in the blade cascade. A jump of entropy is also observed due to the condensation process in the transonic flows in the turbine blades. This indicates that the heat and mass transfer is essential to evaluate the condensation loss of steam in turbine blades considering the changes of the entropy and enthalpy due to the phase change process.

The massive droplets during the nonequilibrium condensation in the blade cascade not only results in the energy loss but also can impact on the blade surface to cause the erosion issue, which both can influence the efficiency and reliability of the steam turbines [57]. To evaluate the energy loss of the steam turbine, the following equation is employed to quantitatively analyse the condensation loss [58, 59].

$$Ldr = q_{dr}(m_{out} - m_{in})h_{fg} \tag{18}$$

where Ldr is the condensation loss, q_{dr} is the condensation loss coefficient, m_{out} and m_{in} are liquid flow rates at the outlet and inlet of blade cascades.

Table 2 describes the condensation loss due to the nonequilibrium condensation inside blade cascades of a steam turbine, including the latent heat, liquid mass flow rate and the condensation loss. It can be found that the formation of the condensed droplets an irreversible process and subsequently can result in condensation losses up to 0.118 MW in this evaluated blade cascade.

Table 2 Condensation loss in the blade cascade of a steam turbine

h_{fg} (kJ/kg)	m_{in} (kg/s)	m_{out} (kg/s)	q_{dr} (-)	L_{dr} (MW)
2304.462	0.00	0.0510	1.00	0.118

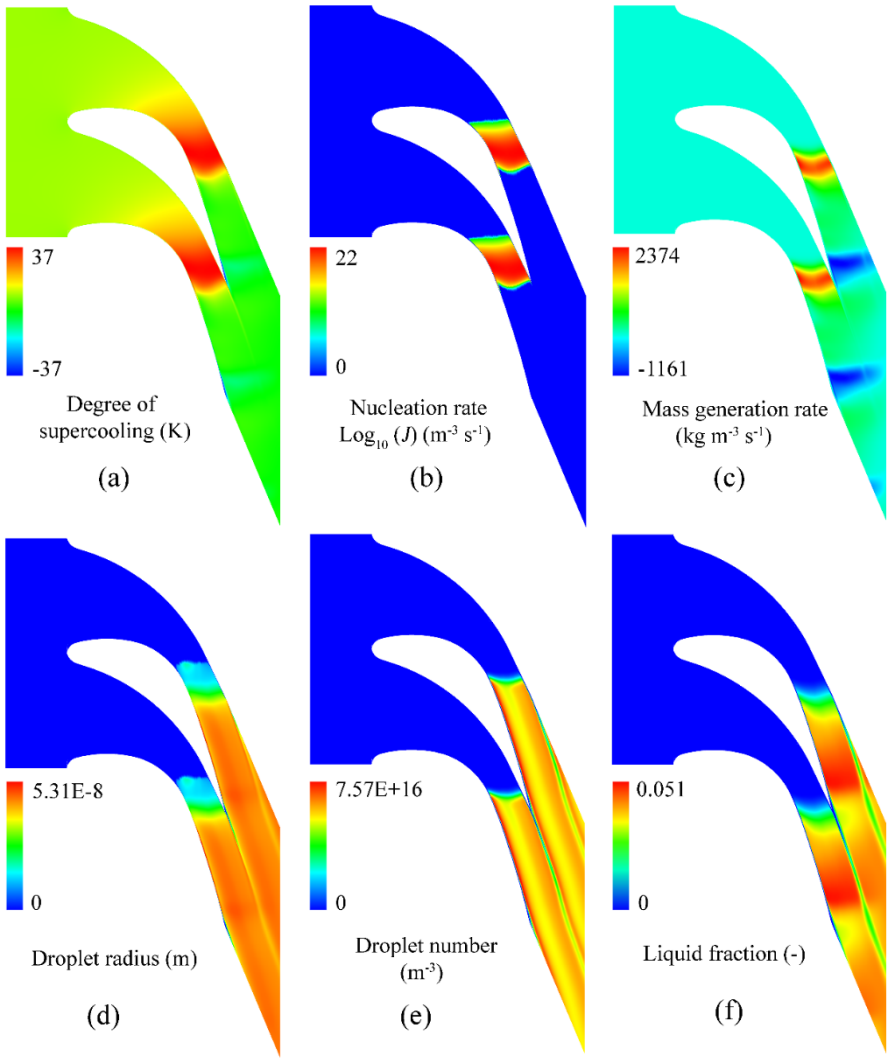

Fig. 8 Non-equilibrium condensation parameters in blade cascades of a steam turbine

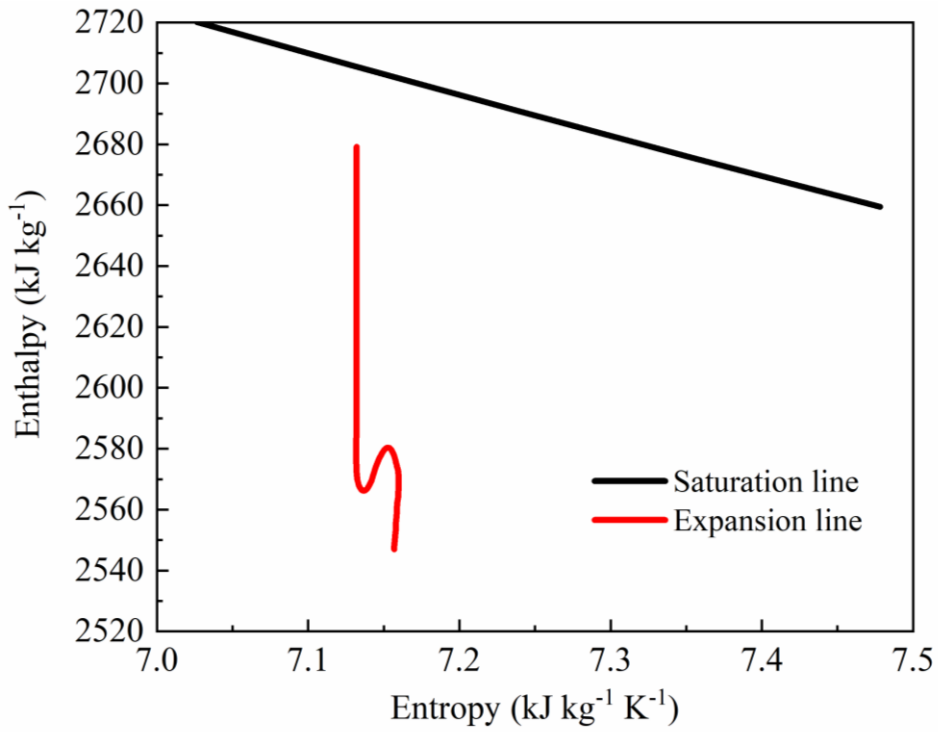

Fig. 9 Entropy-enthalpy at the middle line in the flow region from the inlet to the blade outlet without including the downstream flow channel of the blade cascade

3.4. Effect of trailing edge on wet steam flows in blade cascades

In this section, we evaluate the effect of the cutback of the trailing edge on the blade performance in a steam turbine. The cutback level is defined as the ration of cutting the axial distance to the axial chord of the blade. The wet steam flow structures are analysed in detail based on four different cutbacks of the trailing edge including the original blade, 7%, 14% and 21% cutback, as shown in Fig. 10. The wall pressures on the blade surfaces under four different cutbacks of the trailing edge are illustrated in Fig. 11. It can be seen that the wall pressure of 7% cutback of the trailing edge is almost the same as the ones of the original geometry. When the cutback level of the trailing edge increases to 14% of the blade, the wall pressures on both pressure side and suction side show a slight divergence from the original geometry. The cutback of the trailing

edge by 21% results in dramatic changes of the wall pressure distributions, which significantly diverges from the original operating conditions.

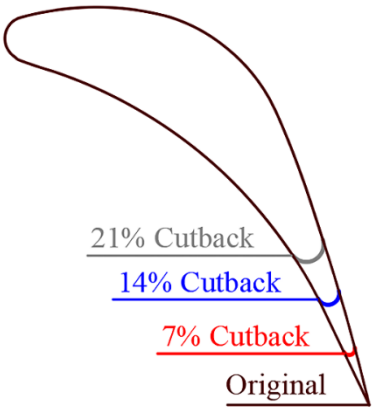

Fig. 10 Strategy of the cutback of the trailing edge of the steam blade

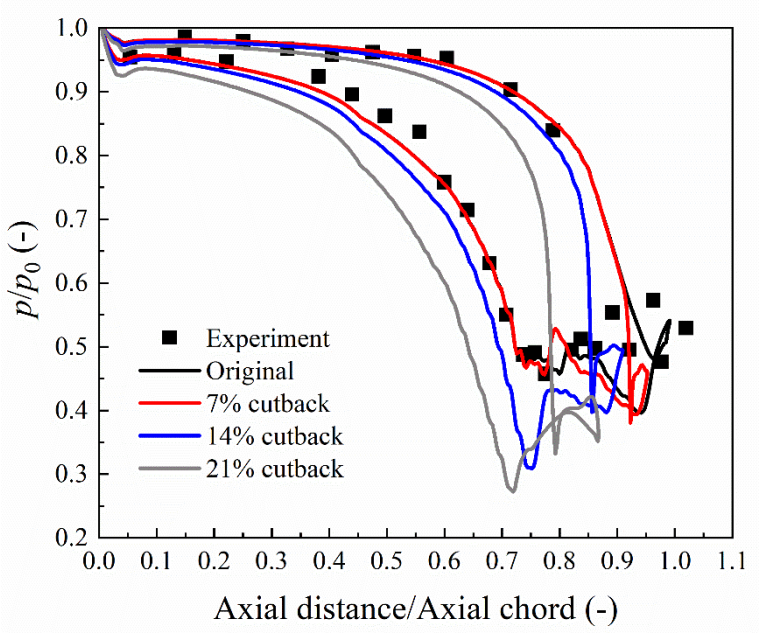

Fig. 11 Wall pressures on the steam blade surface under four different cutbacks of the trailing edge of the steam blade

The static pressure contours, Mach number contours and streamlines under four different cutbacks of the trailing edge of the steam blade are described in Figs. 12 - 14. We can see that the increase of the cutback of the trailing edge induces a stronger expansion of the steam in the blade cascade, which leads to lower static pressures and

higher Mach numbers in the cascades. As shown in Table 3, the Mach number for the original geometry of the trailing edge is about 1.16. The 14% and 21% cutbacks of the trailing edge will result in the increase of the Mach number to 1.44 and 1.52, respectively. In these cases, the interaction between the stronger expansion flow and the blade surface induces more complicated flow structures in the cascades, i.e. the oblique waves become more violent as a result of the increasing cutback of the trailing edge. Combining with the streamlines in Fig. 14, we can see that there is no flow separation both on the pressure side and suction side for the three cases of the original geometry, 7% and 14% cutbacks of the trailing edge, although the vortex flows are observed downstream the trailing edge of the steam blade. On the contrary, the 21% cutback of the trailing edge induces strong flow separations on the suction side of the blade. This indicates that the flow structures severely deteriorate because of the high cutback of the trailing edge and the steam blades will not be working as the original operating conditions.

Table 3 Flow parameters in blade cascades with four cutbacks of trailing edges

Flow parameter	Original	7% Cutback	14% Cutback	21% Cutback
Minimum pressure (Pa)	68153	65528	53103	45115
Max Mach number (-)	1.16	1.28	1.44	1.52
Max droplet radius (μm)	0.0510	0.0491	0.0425	0.0278
Averaged liquid fraction (-)	0.01226	0.01249	0.01277	0.01086

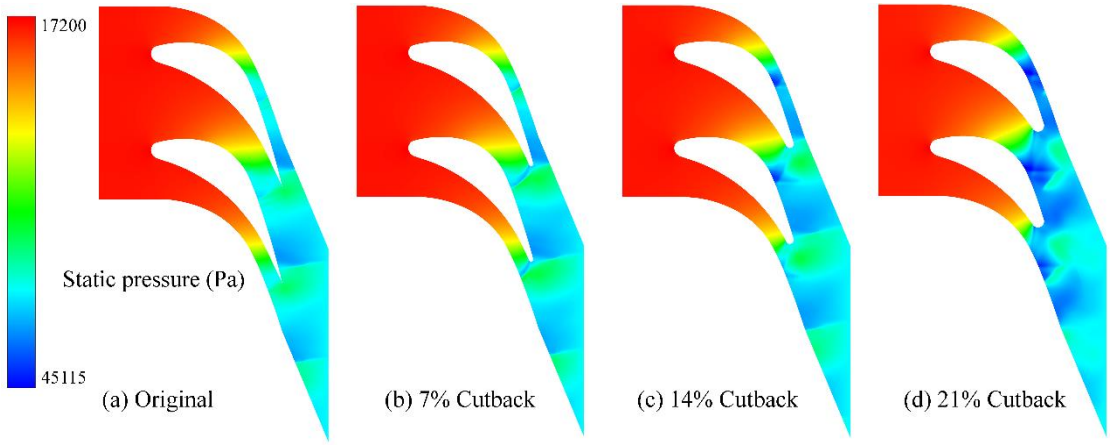

Fig. 12 Static pressure contours under four different cutbacks of the trailing edge of the steam blade

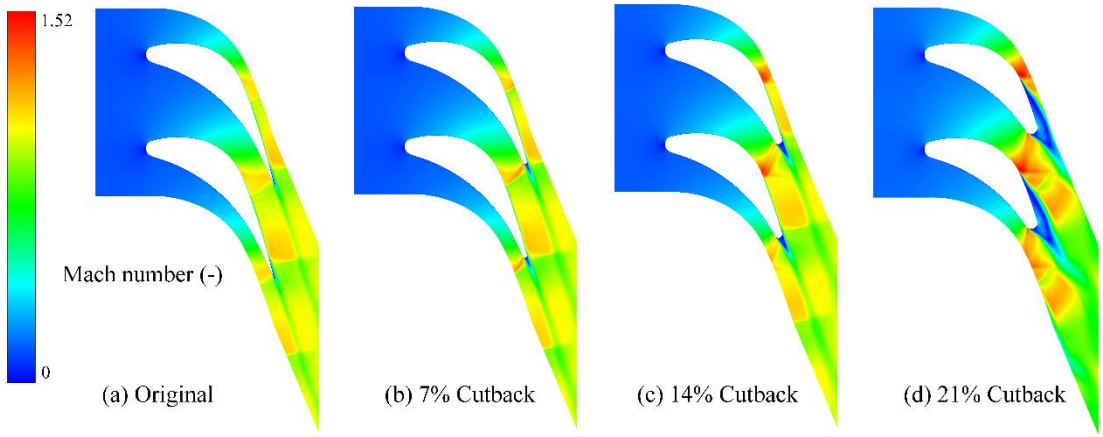

Fig. 13 Mach number contours under four different cutbacks of the trailing edge of the steam blade

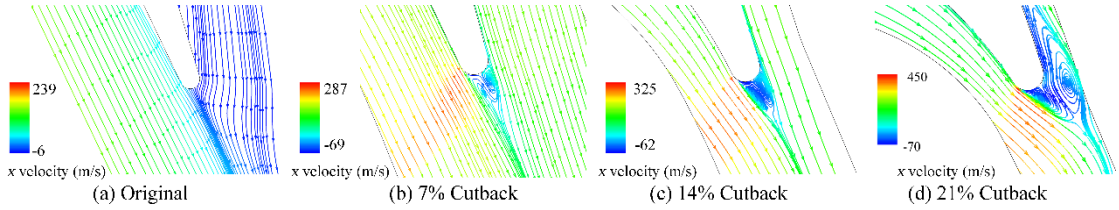

Fig. 14 Streamlines under four different cutbacks of the trailing edge of the steam blade

The nucleation rate contours and profiles at the middle line of the blade cascade under four different geometrical trailing edges are shown in Fig. 15 and Fig .16, respectively. It can be observed that the 14% and 21% cutbacks of the trailing edge

induce an upstream movement of the onset of the homogeneous nucleation. The comparison between the original geometry and 7% cutback of the trailing edge shows that the 7% cutback of the trailing edge narrows the nucleation region in the blade cascade. Fig. 17 and Fig. 18 presents the droplet size and liquid fraction distributions in the blade cascade under different cutback of the trailing edge. Combining the data in Table 3, it is shown that the maximum droplet radius decreases with the increase of the cutback of the trailing edge. For instance, the droplet radius can reach 0.0510 μm for the original blade, which reduces to 0.0278 μm for the 21% cutback case. By comparing the liquid fraction contours of all four cases, we can see that the original, 7% cutback and 14% cutback cases present similar distributions of the liquid phase while the 21% cutback of the trailing edge disturbs the liquid generation due to the violent flow separation in the blade cascade. The averages liquid fraction and condensation loss are shown in Fig. 19 under four different cutbacks of the trailing edge. For original, 7% and 14% cases, the averaged liquid fraction increases with the rise of the increasing cutback of the trailing edge. Due to the flow separation in the 21% cutback case, the liquid region is reduced in the blade cascade and the averaged liquid fraction decreases subsequently compared to the other three cases. Also, the cutback of the trailing edge of the steam blade does not affect significantly the condensation loss which is approximately 0.118 MW for original, 7% and 14% cases. Although the condensation loss for the 21% cutback case reduces to 0.107 MW, the flow separation under this condition will significantly increase the flow losses compared to the other three cases.

In general, the cutback of the trailing edge to 14% is acceptable for the Bakhtar et

al steam blade considering the flow structure, the liquid generation due to the nonequilibrium condensation and the condensation loss. The 21% cutback of the trailing edge induces strong flow separation on the suction side of the steam blade, and the flow structure deteriorate severely in the blade cascades.

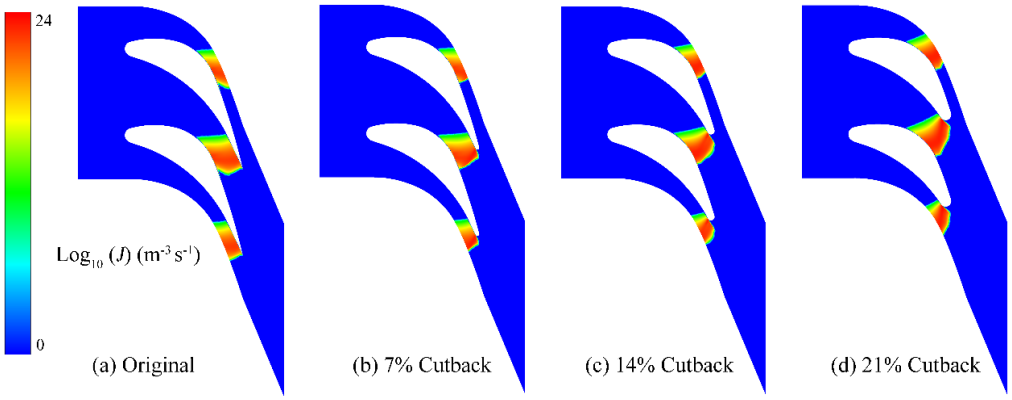

Fig. 15 Nucleation rate contours under four different cutbacks of the trailing edge of the steam blade

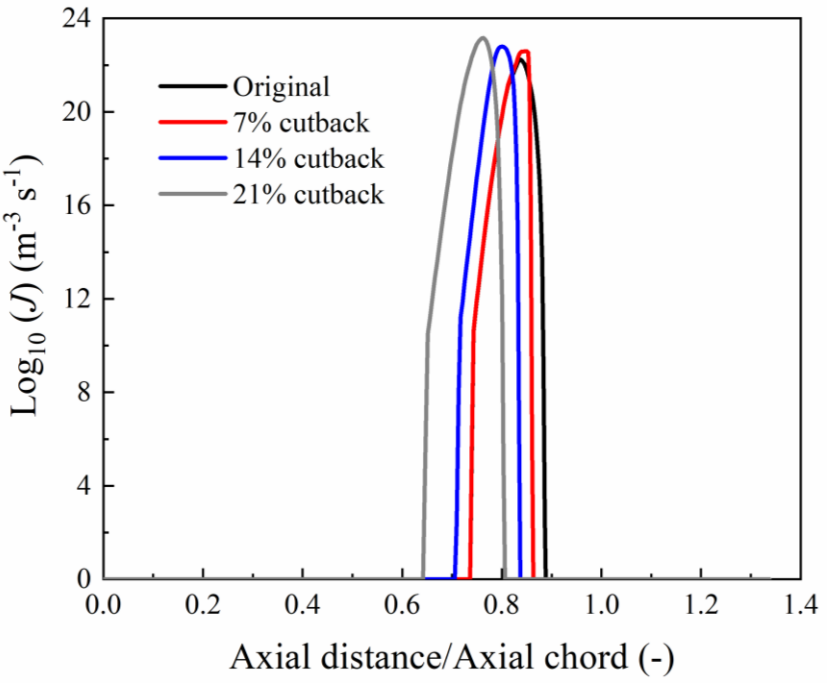

Fig. 16 Nucleation rate profiles at the middle line under four different cutbacks of the trailing edge of the steam blade

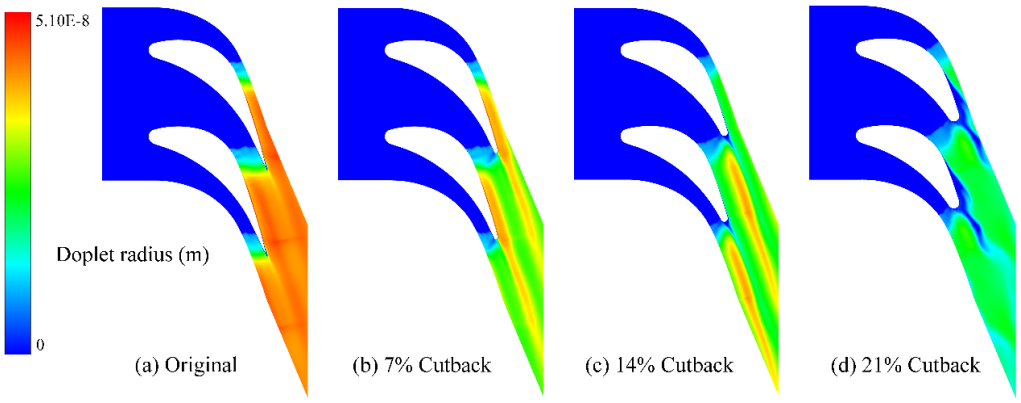

Fig. 17 Droplet radius contours under four different cutbacks of the trailing edge of the steam blade

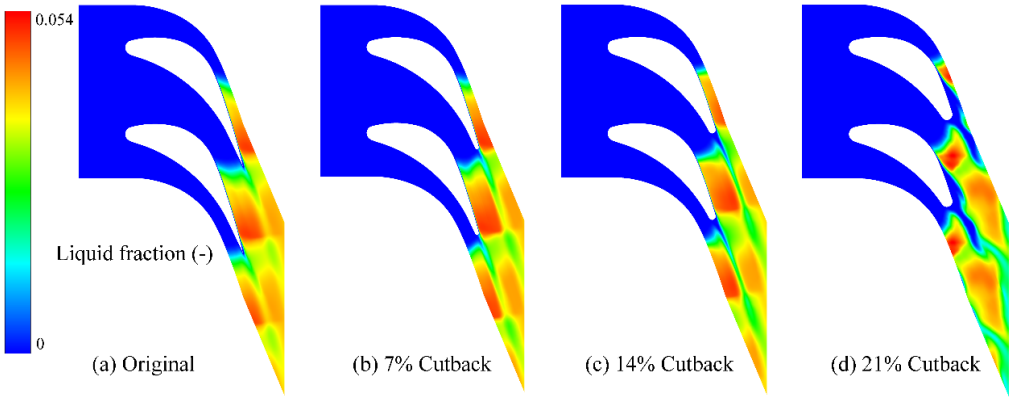

Fig. 18 Liquid fraction contours under four different cutbacks of the trailing edge of the steam blade

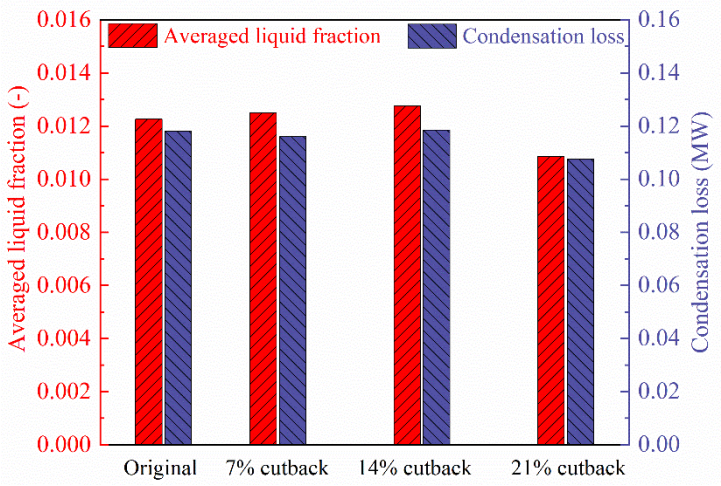

Fig. 19 Average liquid fraction and condensation loss under four different cutbacks of the trailing edge of the steam blade

4. Conclusions

The wet steam modelling is proposed for evaluating the flow behaviour and energy loss inside blade cascades of a steam turbine. The developed computational modelling is validated against the supersonic nozzle flow by comparing the pressure distribution and droplet size, which is further validated against the blade wall pressure and droplet size inside blade cascades. The dry gas model calculates fraudulently flow separations near the trailing edge to induce the complicated oblique waves. The wet steam modelling improves flow structure predictions considering nonequilibrium condensations inside blade cascades. The wet steam modelling predicts the liquid fraction of about 0.051, which can cause a condensation loss of about 0.118 MW in a steam turbine. The increase of the cutback of the trailing edge induces higher expansion flow in the blade cascade as well as leads to the earlier onset of the homogeneous nucleation process. The cutback of the trailing edge by 14% is reasonable to repair the damaged blade considering the flow structure, nonequilibrium phase change and condensation loss. The 21% cutback of the trailing edge results in strong flow separation on the suction side and the flow structures severely deteriorate in the blade cascades, which results in the unacceptable blade performance. This work improves the understanding of the condensation of the steam and evaporation of the condensed droplets in transonic flows in the steam turbine.

The two-dimensional simulation is performed in this study to evaluate the performance of the turbine blade considering the nonequilibrium condensation. If the real three-dimensional flows in the rotor blade cascade are considered, different

expansion ratios would be present along with the blade height. As a consequence, it would be a great challenging to play with correction factors in the wet steam model, which needs to be clarified in future studies.

Conflict of interest

The authors declared that there is no conflict of interest.

Acknowledgements

This project has received funding from the European Union's Horizon 2020 research and innovation programme under the Marie Sklodowska-Curie grant agreement No 792876 and No 778104, and the National Natural Science Foundation of China under Grant 51876143.

References

[1] M.A.F. Aliabadi, E. Lakzian, I. Khazaei, A. Jahangiri, A comprehensive investigation of finding the best location for hot steam injection into the wet steam turbine blade cascade, Energy, 190 (2020) 116397.

[2] S.N.R. Abadi, A. Ahmadpour, S. Abadi, J.P. Meyer, CFD-based shape optimization of steam turbine blade cascade in transonic two phase flows, Applied Thermal Engineering, 112 (2017) 1575-1589.

[3] H.B. Esfe, M. Kermani, M.S. Avval, Effects of surface roughness on deviation angle and performance losses in wet steam turbines, Applied Thermal Engineering, 90 (2015) 158-173.

[4] F. Bakhtar, Z. Mamat, O. Jadayel, M.R. Mahpeykar, On the performance of a cascade of improved turbine nozzle blades in nucleating steam. Part 1: surface

pressure distributions, Proceedings of the Institution of Mechanical Engineers, Part C: Journal of Mechanical Engineering Science, 223 (2009) 1903-1914.

[5] F. Bakhtar, H. Mashmoushy, O. Jadayel, On the performance of a cascade of turbine rotor tip section blading in wet steam part 2: surface pressure distributions, Proceedings of the Institution of Mechanical Engineers, Part C: Journal of Mechanical Engineering Science, 211 (1997) 531-540.

[6] F. Bakhtar, S. Rassam, G. Zhang, On the performance of a cascade of turbin rotor tip section blading in wet steam Part 4: Droplet measurements, Proceedings of the Institution of Mechanical Engineers, Part C: Journal of Mechanical Engineering Science, 213 (1999) 343-353.

[7] A. White, J. Young, P. Walters, Experimental validation of condensing flow theory for a stationary cascade of steam turbine blades, Philosophical Transactions of the Royal Society of London. Series A: Mathematical, Physical and Engineering Sciences, 354 (1996) 59-88.

[8] A.H. Yousif, A.M. Al-Dabagh, R.C. Al-Zuhairy, Non-equilibrium spontaneous condensation in transonic steam flow, International Journal of Thermal Sciences, 68 (2013) 32-41.

[9] S. Dykas, M. Majkut, M. Strozik, K. Smołka, Losses estimation in transonic wet steam flow through linear blade cascade, Journal of Thermal Science, 24 (2015) 109-116.

[10] W. Wróblewski, S. Dykas, A. Gardzilewicz, M. Kolovratnik, Numerical and Experimental Investigations of Steam Condensation in LP Part of a Large Power

Turbine, Journal of Fluids Engineering, 131 (2009).

[11] S. Dykas, M. Majkut, K. Smołka, M. Strozik, Analysis of the steam condensing flow in a linear blade cascade, Proceedings of the Institution of Mechanical Engineers, Part A: Journal of Power and Energy, 232 (2018) 501-514.

[12] A. Ebrahimi-Fizik, E. Lakzian, A. Hashemian, Entropy generation analysis of wet-steam flow with variation of expansion rate using NURBS-based meshing technique, International Journal of Heat and Mass Transfer, 139 (2019) 399-411.

[13] A. Hashemian, E. Lakzian, A. Ebrahimi-Fizik, On the application of isogeometric finite volume method in numerical analysis of wet-steam flow through turbine cascades, Computers & Mathematics with Applications, 79 (2020) 1687-1705.

[14] F. Bakhtar, M. Zamri, J. Rodriguez-Lelis, A comparative study of treatment of two-dimensional two-phase flows of steam by a Runge-Kutta and by Denton's methods, Proceedings of the Institution of Mechanical Engineers, Part C: Journal of Mechanical Engineering Science, 221 (2007) 689-706.

[15] W. Wróblewski, S. Dykas, A. Gepert, Steam condensing flow modeling in turbine channels, International Journal of Multiphase Flow, 35 (2009) 498-506.

[16] H. Ding, Y. Li, E. Lakzian, C. Wen, C. Wang, Entropy generation and exergy destruction in condensing steam flow through turbine blade with surface roughness, Energy Conversion and Management, 196 (2019) 1089-1104.

[17] M. Vatanmakan, E. Lakzian, M.R. Mahpeykar, Investigating the entropy generation in condensing steam flow in turbine blades with volumetric heating, Energy, 147 (2018) 701-714.

[18] G. Zhang, L. Wang, S. Zhang, Y. Li, Z. Zhou, Effect evaluation of a novel dehumidification structure based on the modified model, Energy Conversion and Management, 159 (2018) 65-75.

[19] G. Zhang, F. Wang, D. Wang, T. Wu, X. Qin, Z. Jin, Numerical study of the dehumidification structure optimization based on the modified model, Energy Conversion and Management, 181 (2019) 159-177.

[20] G. Zhang, X. Zhang, F. Wang, D. Wang, Z. Jin, Z. Zhou, Numerical investigation of novel dehumidification strategies in nuclear plant steam turbine based on the modified nucleation model, International Journal of Multiphase Flow, 120 (2019) 103083.

[21] G. Zhang, X. Zhang, F. Wang, D. Wang, Z. Jin, Z. Zhou, Design and optimization of novel dehumidification strategies based on modified nucleation model in three-dimensional cascade, Energy, 187 (2019) 115982.

[22] S. Dykas, W. Wróblewski, Two-fluid model for prediction of wet steam transonic flow, International Journal of Heat and Mass Transfer, 60 (2013) 88-94.

[23] X. Han, W. Zeng, Z. Han, Investigating the dehumidification characteristics of the low-pressure stage with blade surface heating, Applied Thermal Engineering, 164 (2020) 114538.

[24] A. Ebrahimi-Fizik, E. Lakzian, A. Hashemian, Numerical investigation of wet inflow in steam turbine cascades using NURBS-based mesh generation method, International Communications in Heat and Mass Transfer, 118 (2020) 104812.

[25] L. Cao, J. Wang, H. Luo, H. Si, R. Yang, Distribution of condensation droplets in

the last stage of steam turbine under small flow rate condition, Applied Thermal Engineering, 181 (2020) 116021.

[26] S. Yazdani, E. Lakzian, Numerical simulation and passive control of condensing flow through turbine blade by NVD Method Using Eulerian–Lagrangian Model, Computers & Mathematics with Applications, 80 (2020) 140-160.

[27] H. Ding, Y. Tian, C. Wen, C. Wang, C. Sun, Polydispersed droplet spectrum and exergy analysis in wet steam flows using method of moments, Applied Thermal Engineering, 182 (2021) 116148.

[28] S. Moriguchi, H. Miyazawa, T. Furusawa, S. Yamamoto, Large eddy simulation of a linear turbine cascade with a trailing edge cutback, Energy, 220 (2021) 119694.

[29] C. Wen, N. Karvounis, J.H. Walther, H. Ding, Y. Yang, Non-equilibrium condensation of water vapour in supersonic flows with shock waves, International Journal of Heat and Mass Transfer, 149 (2020) 119109.

[30] J. Bian, X. Cao, W. Yang, X. Song, C. Xiang, S. Gao, Condensation characteristics of natural gas in the supersonic liquefaction process, Energy, 168 (2019) 99-110.

[31] C. Wen, N. Karvounis, J.H. Walther, Y. Yan, Y. Feng, Y. Yang, An efficient approach to separate CO2 using supersonic flows for carbon capture and storage, Applied Energy, 238 (2019) 311-319.

[32] H. Ding, C. Wang, C. Chen, Non-equilibrium condensation process of water vapor in moist air expansion through a sonic nozzle, Flow Measurement and Instrumentation, 40 (2014) 238-246.

[33] C. Wen, H. Ding, Y. Yang, Performance of steam ejector with nonequilibrium

condensation for multi-effect distillation with thermal vapour compression (MED-TVC) seawater desalination system, Desalination, 489 (2020) 114531.

[34] J. Bian, X. Cao, W. Yang, D. Guo, C. Xiang, Prediction of supersonic condensation process of methane gas considering real gas effects, Applied Thermal Engineering, 164 (2020) 114508.

[35] J. Bian, X. Cao, W. Yang, M.A. Edem, P. Yin, W. Jiang, Supersonic liquefaction properties of natural gas in the Laval nozzle, Energy, 159 (2018) 706-715.

[36] A. Kantrowitz, Nucleation in very rapid vapor expansions, The Journal of Chemical Physics, 19 (1951) 1097-1100.

[37] J. Young, The spontaneous condensation of steam in supersonic nozzle, Physico Chemical Hydrodynamics, 3 (1982) 57-82.

[38] J. Starzmann, F.R. Hughes, S. Schuster, A.J. White, J. Halama, V. Hric, M. Kolovratník, H. Lee, L. Sova, M. Št'astný, M. Grübel, M. Schatz, D.M. Vogt, Y. Patel, G. Patel, T. Turunen-Saaresti, V. Gribin, V. Tishchenko, I. Gavrilov, C. Kim, J. Baek, X. Wu, J. Yang, S. Dykas, W. Wróblewski, S. Yamamoto, Z. Feng, L. Li, Results of the International Wet Steam Modeling Project, Proceedings of the Institution of Mechanical Engineers, Part A: Journal of Power and Energy, 232 (2018) 550-570.

[39] E. Lemmon, M. Huber, M. McLinden, NIST Standard Reference Database 23: Reference Fluid Thermodynamic and Transport Properties-REFPROP, Version 9.1, May 7, 2013., in.

[40] T. Furusawa, S. Yamamoto, Mathematical modeling and computation of high-

pressure steam condensation in a transonic flow, Journal of Fluid Science and Technology, 12 (2017) JFST0002.

[41] C. Wen, L. Gong, H. Ding, Y. Yang, Steam ejector performance considering phase transition for multi-effect distillation with thermal vapour compression (MED-TVC) desalination system, Applied Energy, 279 (2020) 115831.

[42] C. Wen, H. Ding, Y. Yang, Optimisation study of a supersonic separator considering nonequilibrium condensation behaviour, Energy Conversion and Management, 222 (2020) 113210.

[43] A. Jarrahian, E. Heidaryan, A new cubic equation of state for sweet and sour natural gases even when composition is unknown, Fuel, 134 (2014) 333-342.

[44] A. Jarrahian, E. Heidaryan, A simple correlation to estimate natural gas viscosity, Journal of Natural Gas Science and Engineering, 20 (2014) 50-57.

[45] A. Jarrahian, H.R. Karami, E. Heidaryan, On the isobaric specific heat capacity of natural gas, Fluid Phase Equilibria, 384 (2014) 16-24.

[46] A. Jarrahian, E. Heidaryan, A simple correlation to estimate natural gas thermal conductivity, Journal of Natural Gas Science and Engineering, 18 (2014) 446-450.

[47] F.R. Menter, Two-equation eddy-viscosity turbulence models for engineering applications, AIAA journal, 32 (1994) 1598-1605.

[48] C. Wen, B. Rogie, M.R. Kærn, E. Rothuizen, A first study of the potential of integrating an ejector in hydrogen fuelling stations for fuelling high pressure hydrogen vehicles, Applied Energy, 260 (2020) 113958.

[49] Y. Yang, X. Zhu, Y. Yan, H. Ding, C. Wen, Performance of supersonic steam

ejectors considering the nonequilibrium condensation phenomenon for efficient energy utilisation, Applied Energy, 242 (2019) 157-167.

[50] S. Dykas, W. Wróblewski, Numerical modelling of steam condensing flow in low and high-pressure nozzles, International Journal of Heat and Mass Transfer, 55 (2012) 6191-6199.

[51] F. Bakhtar, M.R. Mahpeykar, K.K. Abbas, An Investigation of Nucleating Flows of Steam in a Cascade of Turbine Blading-Theoretical Treatment, Journal of Fluids Engineering, 117 (1995) 138-144.

[52] M.J. Moore, P.T. Walters, R.I. Crane, B.J. Davidson, Predicting the Fog-drop Size in Wet-Steam Turbines, Proc. of IMECHE Conf. Wet Steam 4, Coventry, UK, (1973).

[53] H. Gürbüz, D. Buran, Experimental study on the effect of concentrated turbulence around the spark plug zone in a swirling flow on a hydrogen SI engine performance and combustion parameters, Journal of Energy Engineering, 142 (2016) 04015031.

[54] H. Gürbüz, Experimental evaluation of combustion parameters with ion-current sensor integrated to fast response thermocouple in SI engine, Journal of Energy Engineering, 143 (2017) 04016046.

[55] Ö. Solmaz, H. Gürbüz, M. Karacor, Comparison of Artificial Neural Network and Fuzzy Logic Approaches for the Prediction of In-Cylinder Pressure in a Spark Ignition Engine, Journal of Dynamic Systems, Measurement, and Control, 142 (2020) 091005.

[56] C. Wen, H. Ding, Y. Yang, Numerical simulation of nanodroplet generation of

water vapour in high-pressure supersonic flows for the potential of clean natural gas dehydration, Energy Conversion and Management, 231 (2021) 113853.

[57] S. Dykas, M. Majkut, K. Smołka, M. Strozik, Study of the wet steam flow in the blade tip rotor linear blade cascade, International Journal of Heat and Mass Transfer, 120 (2018) 9-17.

[58] H. Kawagishi, A. Onoda, N. Shibukawa, Y. Niizeki, Development of moisture loss models in steam turbines, Heat Transfer—Asian Research, 42 (2013) 651-664.

[59] M.A.F. Aliabadi, E. Lakzian, A. Jahangiri, I. Khazaei, Numerical investigation of effects polydispersed droplets on the erosion rate and condensation loss in the wet steam flow in the turbine blade cascade, Applied Thermal Engineering, 164 (2020) 114478.